

**DETC2005-85376**

## **MODELING THE TRANSIENT AND STEADY-STATE FLOW OVER A STATIONARY CYLINDER**

**Ali H. Nayfeh,\* Osama A. Marzouk, Haider N. Arafat, Imran Akhtar**

Department of Engineering Science and Mechanics, MC 0219  
Virginia Polytechnic Institute and State University  
Blacksburg, Virginia, 24061

Email: anayfeh@vt.edu, omarzouk@vt.edu, harafat@vt.edu, akhtar@vt.edu

### **ABSTRACT**

*A reduced-order model for the two-dimensional flow over a stationary circular cylinder is examined. The lift is modeled with the van der Pol equation with three parameters; it models self-excited self-limiting systems. The drag is modeled as the sum of a mean term and a time-varying term proportional to the product of the lift and its time derivative. The transient and steady-state flows are calculated using a CFD code based on the unsteady Reynolds-averaged Navier-Stokes equations. The steady-state lift and drag CFD results are used to identify the three parameters in the lift model using a combination of higher-order spectral techniques and perturbation methods. The model is validated using steady-state numerical simulations for three cases describing low, moderate, and high Reynolds number flows. Then, the model is shown to reproduce the transient lift and drag calculated with the CFD code.*

### **INTRODUCTION**

The flow around a circular cylinder has been the subject of intense research mostly by experiments [1–4] and also by using numerical simulations [5–8]. In addition to being a building block in the understanding of the flow over bluff bodies, it has many applications in several engineering branches. Vortex-induced vibration (VIV) of structures is of practical interest in many engineering problems and the prediction of VIV has received a wide interest by experimental, analytical, and numerical

researchers [9–11]. Experimental studies of such structures are quite costly and often not feasible. Modeling of VIV of circular cylinders is of particular interest in offshore oil production riser systems. These vibrations involve complicated nonlinear interactions between the cylinder motions and the fluid forces, the lift and drag forces. The cylinder motion and fluid forces can affect each other and may lead to resonance. An ultimate solution for this problem would be a time-domain numerical simulation of the fluid flow and the cylinder response, including elastic effects. In this solution, the fluid and the cylinder would be treated as a single dynamical system and all of the governing equations would be solved simultaneously and interactively in the time domain. Obviously, this is a formidable task, especially when considering the fact that the Reynolds numbers associated with full-scale flows in oil production riser systems are quite large. Alternatively, one could construct a model that takes into consideration all of the physical aspects, yet capable of predicting the VIV.

A well-known model for the lift force acting on a circular cylinder in a uniform flow field is the lift wake oscillator proposed by Hartlen and Currie [12]. In this model, the lift is represented by the Rayleigh equation. Currie and Turnbull [13] proposed a similar model for the fluctuations of the drag coefficient. Iwan and Blevins [14] also used the Rayleigh equation to model the fluctuating lift, but assumed that the force coupling the structure and fluid depends only on the relative velocity and acceleration of the flow. Skop and Griffin [15] introduced a modified van der Pol lift model that includes an additional term, which is

---

\*Address all correspondence to this author.

cubic in the lift. Skop and Balasubramanian [16] used the van der Pol equation with a parametric nonlinear coupling forcing, whose form is constructed based on the experimental synchronization results of Williamson and Roshko [4]. Skop and Balasubramanian [17] also extended their model to the problem of shear flows by adding an axial diffusion term. Billah and Ahmad [18] also considered the VIV problem of a cylinder under a parametric excitation.

To investigate vortex-induced vibrations of flexible cylindrical structures, Skop and Balasubramanian [19] assumed that the fluctuating lift is comprised of two parts. They modeled one part with the van der Pol equation and the second by a “stall” term proportional to the cylinder velocity. Kim and Perkins [20] modeled the lift and drag by two nonlinearly coupled van der Pol equations in their study of resonant responses of suspended elastic cables. The coupling terms were introduced based on the fact that the main frequency of the drag component is twice the main frequency of the lift component.

Most of the aforementioned analytical works are based on modeling the lift by either the Rayleigh or the van der Pol oscillator. Nayfeh et al. [21] numerically simulated the two-dimensional flow past a stationary cylinder for a wide range of Reynolds numbers. By integrating the pressure, they calculated the lift and drag. They employed higher-order spectral analysis to determine the phase relations among the different spectral components of the lift. Then, they compared the CFD obtained phase information with those obtained from closed-form approximate solutions of the van der Pol and Rayleigh oscillators. They concluded that the van der Pol oscillator is the more accurate representation of the lift. They also proposed to model the drag as the sum of a mean term and a time-varying term proportional to the product of the lift and its time derivative.

In all of the previous models, the emphasis is on reproducing the steady-state lift and drag. However, to investigate the fluid-structure interaction more thoroughly requires modeling of the transient as well as the steady-state lift and drag. In the current study, we extend the work of Nayfeh et al. [21] by investigating the validity of their model in the transient region. In other words, is the model identified based on the steady-state lift and drag capable of reproducing the transient lift and drag obtained with the CFD code? We examine this question for three cases representing low, moderate, and high Reynolds number flows. Furthermore, by extending the perturbation analysis to second order, we show that the frequency in the van der Pol equation is not exactly equal to the shedding frequency, but that there exists a slight shift between them.

## NUMERICAL SIMULATION OF THE VORTEX SHEDDING

Direct numerical simulation (DNS) of flows with engineering relevance remains a challenging task even with current ad-

vances in hardware and software capabilities. Hence, some type of modeling or approximation is introduced to simplify the flow computations and make them feasible on existing computer platforms. Usually, the approximation is introduced in the representation of the turbulent scales in the form of a turbulence model, which significantly reduces the spatial and temporal resolution requirements. An alternative to DNS is the large-eddy simulation (LES) approach, which resolves the energy-containing turbulent scales while modeling the subgrid scales (SGS). LES provides information about a wide range of spatial and temporal scales in the flow at a cost that is significantly lower than DNS. However, LES computations of high Reynolds number flows with complex geometries remain a formidable task. In the conventional Reynolds-averaged Navier Stokes (RANS) modeling, which is used extensively in the engineering community, the model represents the effect of all of the turbulent fluctuations. Such a modeling approach with its variants is much cheaper in terms of computation cost than DNS and LES, yet it is an accurate, efficient analysis tool.

The unsteady RANS equations are solved numerically using the artificial compressibility method. This method couples the continuity and momentum equations by adding an artificial time derivative of the pressure term to the continuity equation. Without this term, there is no coupling between the pressure and the velocity and convergence can be remarkably slow. For turbulent closure, the Spalart-Allmaras (SA) method [22,23] is used to model the turbulent fluctuations. The equations are solved on a non-uniform structured grid using a second-order finite-difference scheme. The convective terms are discretized using a second-order upwinding difference scheme. The physical time terms, which represent flow unsteadiness, are switched to the right-hand side and used as source terms; they are discretized using a second-order three-point backward-difference formula. Different boundary conditions are used in the simulations, including inflow, outflow, and no-slip. All of the boundary conditions are treated implicitly in the code to reduce the restriction on the time step and to increase its stability. At the inflow boundary, the velocity components are specified, while the pressure is extrapolated from the interior points. At the outflow boundary, the pressure is specified, whereas the velocity components are extrapolated from the computation domain. In addition, similar boundary conditions are set for the turbulence quantities. The numerical solution provides the pressure distribution over the surface, which is integrated to determine the lift and drag forces over the cylinder. These fluid forces are the input to our reduced-order model.

## SUGGESTED LIFT MODEL

In a previous work, Nayfeh et al. [21] investigated two wake-oscillator models for modeling the lift force, namely, the van der Pol and Rayleigh oscillators. By examining the steady-state lift

data they obtained from the numerical simulation, they found out that the lift force is always composed of the odd components of the *shedding frequency*  $f_s$ , such as  $f_s$  and  $3f_s$ . This is illustrated in Fig. 1, where we present the time histories and spectra of the lift and drag coefficients for a flow at  $Re=10,000$ . In addition to the component with amplitude  $a_1$  at the shedding frequency  $f_s$ , the lift spectrum clearly shows a non-negligible contribution with amplitude  $a_3$  at the harmonic  $3f_s$ .

In addition, using higher-order spectral moments analysis, Nayfeh et al. [21] found that the phase angle between the lift components  $3f_s$  and  $f_s$  is approximately  $270^\circ$ , which means that only the van der Pol oscillator can be used to represent the lift. So, the van der Pol model was deemed to be an efficient but simple tool to model the lift in the steady-state regime.

Here, we show that this capability extends to the transient part of the lift. The van der Pol equation in terms of the lift coefficient  $C_L(t)$  is

$$\ddot{C}_L + \omega^2 C_L = \mu \dot{C}_L - \alpha C_L^2 \dot{C}_L \quad (1)$$

where  $\omega$  is related (but not equal) to the angular shedding frequency  $\omega_s = 2\pi f_s$  and  $\mu$  and  $\alpha$  represent the linear and nonlinear damping coefficients, respectively. The values of  $\mu$  and  $\alpha$  are positive, so that the linear damping is negative and the nonlinear damping is positive. As a result, small disturbances grow and large ones decay, both eventually approaching a stable limit cycle. These parameters change with the Reynolds number  $Re$ .

### Analytical Solution of the van der Pol Equation

We consider the problem when the damping and nonlinearity are weak; that is, we take  $\mu = O(\varepsilon)$  and  $\alpha = O(\varepsilon)$  in Eqn. (1) where  $\varepsilon \ll 1$  is a bookkeeping parameter. We use the method of multiple scales [24,25] to determine a second-order approximate solution in  $\varepsilon$  for the lift coefficient. To this end, we transform Eqn. (1) into a complex-valued first-order equation using the transformation

$$C_L(t) = \zeta(t) + \bar{\zeta}(t) \quad (2)$$

subject to the constraint

$$\frac{dC_L(t)}{dt} = i\omega[\zeta(t) - \bar{\zeta}(t)] \quad (3)$$

Solving Eqns. (2) and (3) for  $\zeta$  and  $\bar{\zeta}$  yields

$$\zeta(t) = \frac{1}{2} \left( C_L - \frac{i}{\omega} \frac{dC_L}{dt} \right) \quad \text{and} \quad \bar{\zeta}(t) = \frac{1}{2} \left( C_L + \frac{i}{\omega} \frac{dC_L}{dt} \right) \quad (4)$$

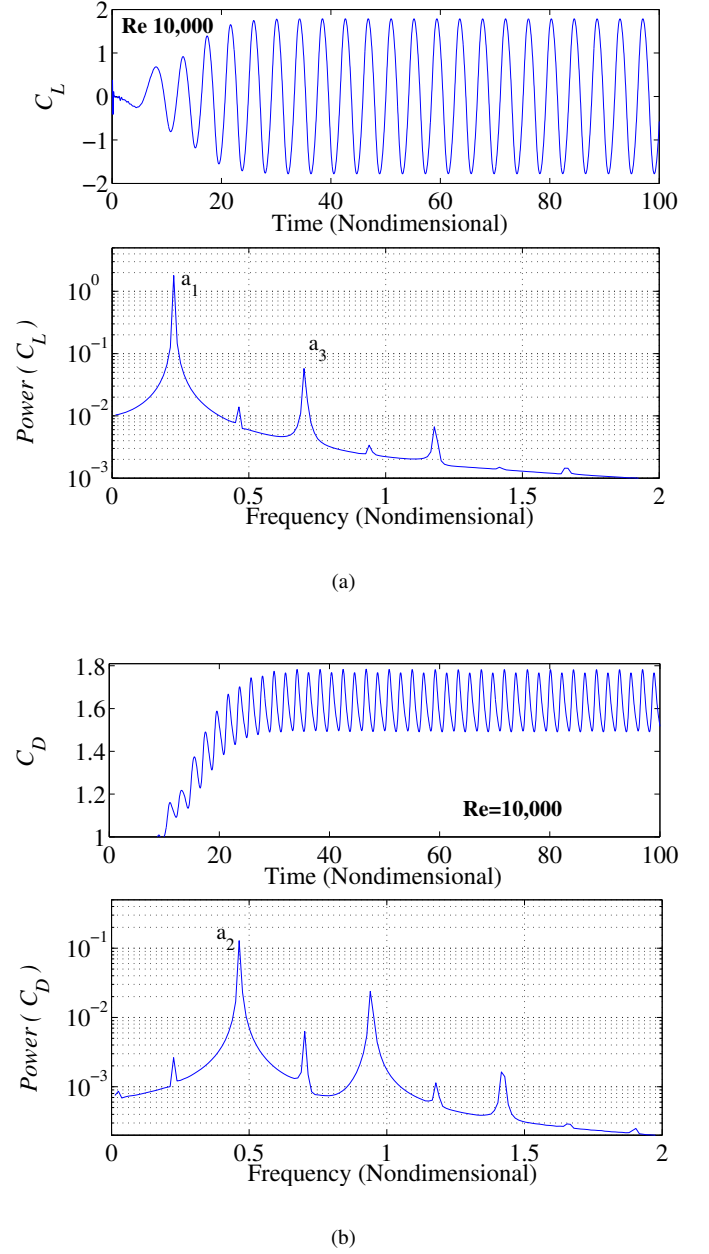


Figure 1. Time histories and spectra of the (a) lift and (b) drag coefficients as obtained from the CFD simulation at  $Re = 10,000$ .

Then, differentiating the first of Eqns. (4) and using Eqns. (1)-(3), we obtain the following first-order complex-valued equation:

$$\dot{\zeta} = i\omega\zeta + \varepsilon \frac{1}{2} \mu (\zeta - \bar{\zeta}) - \varepsilon \frac{1}{2} \alpha (\zeta^3 + \zeta^2 \bar{\zeta} - \zeta \bar{\zeta}^2 - \bar{\zeta}^3) \quad (5)$$

Next, we introduce the fast, slow, and slower time scales  $T_0 = t$ ,  $T_1 = \varepsilon t$ , and  $T_2 = \varepsilon^2 t$ , respectively, and expand  $\zeta$  in the form

$$\zeta = \sum_{j=0}^2 \varepsilon^j \zeta_j(T_0, T_1, T_2) + O(\varepsilon^3) \quad (6)$$

In terms of these time scales, the time derivative becomes  $d/dt = D_0 + \varepsilon D_1 + \varepsilon^2 D_2 + \dots$ , where  $D_j = \partial/\partial T_j$ . Substituting Eqns. (6) and its complex conjugate into Eqn. (5) and separating coefficients of like powers of  $\varepsilon$ , we obtain

$$D_0 \zeta_0 - i\omega \zeta_0 = 0 \quad (7)$$

$$D_0 \zeta_1 - i\omega \zeta_1 = -D_1 \zeta_0 + \frac{1}{2} \mu (\zeta_0 - \bar{\zeta}_0) - \frac{1}{2} \alpha (\zeta_0^3 + \zeta_0^2 \bar{\zeta}_0 - \zeta_0 \bar{\zeta}_0^2 - \bar{\zeta}_0^3) \quad (8)$$

$$D_0 \zeta_2 - i\omega \zeta_2 = -D_2 \zeta_0 - D_1 \zeta_1 + \frac{1}{2} \mu (\zeta_1 - \bar{\zeta}_1) - \frac{3}{2} \alpha (\zeta_0^2 \zeta_1 - \bar{\zeta}_0^2 \bar{\zeta}_1) + \frac{1}{2} \alpha (\bar{\zeta}_0^2 \zeta_1 - \zeta_0^2 \bar{\zeta}_1) - \alpha (\zeta_0 \bar{\zeta}_0 \zeta_1 - \zeta_0 \bar{\zeta}_0 \bar{\zeta}_1) \quad (9)$$

The solution of Eqn. (7) is

$$\zeta_0(T_0, T_1, T_2) = A(T_1, T_2) e^{i\omega T_0} \quad (10)$$

Substituting Eqn. (10) into Eqn. (8) yields

$$D_0 \zeta_1 - i\omega \zeta_1 = \left( \frac{\mu}{2} A - \frac{\alpha}{2} A^2 \bar{A} - \frac{\partial A}{\partial T_1} \right) e^{i\omega T_0} - \frac{\alpha}{2} A^3 e^{3i\omega T_0} - \left( \frac{\mu}{2} \bar{A} - \frac{\alpha}{2} A \bar{A}^2 \right) e^{-i\omega T_0} + \frac{\alpha}{2} \bar{A}^3 e^{-3i\omega T_0} \quad (11)$$

Eliminating the terms that lead to secular terms (i.e., the terms proportional to  $e^{i\omega T_0}$ ) from Eqn. (11) yields the solvability condition

$$\frac{\partial A}{\partial T_1} = \frac{1}{2} \mu A - \frac{1}{2} \alpha A^2 \bar{A} \quad (12)$$

Then, the solution of Eqn. (11) becomes

$$\zeta_1(T_0, T_1, T_2) = -\frac{i}{4\omega} (\mu \bar{A} - \alpha A \bar{A}^2) e^{-i\omega T_0} + \frac{i\alpha}{4\omega} A^3 e^{3i\omega T_0} + \frac{i\alpha}{8\omega} \bar{A}^3 e^{-3i\omega T_0} \quad (13)$$

Substituting for  $\zeta_0$  and  $\zeta_1$  in Eqn. (9) and eliminating the secular terms leads to the second solvability condition

$$\frac{\partial A}{\partial T_2} = -\frac{i}{16\omega} (2\mu^2 A - 12\alpha\mu A^2 \bar{A} + 11\alpha^2 A^3 \bar{A}^2) \quad (14)$$

To obtain the final solution, we substitute Eqns. (10) and (13) into Eqn. (6) and obtain

$$\zeta(T_0, T_1, T_2) = A e^{i\omega T_0} + \varepsilon \frac{i}{4\omega} \left[ (\alpha A \bar{A}^2 - \mu \bar{A}) e^{-i\omega T_0} + \alpha A^3 e^{3i\omega T_0} + \frac{1}{2} \alpha \bar{A}^3 e^{-3i\omega T_0} \right] + O(\varepsilon^2) \quad (15)$$

Then, we substitute Eqn. (15) into Eqn. (2), replace the  $T_n$  with  $\varepsilon^n t$ , and obtain

$$C_L(t) = A e^{i\omega t} + \bar{A} e^{-i\omega t} - \varepsilon \frac{i}{4\omega} \left[ (\alpha A^2 \bar{A} - \mu A) e^{i\omega t} - (\alpha A \bar{A}^2 - \mu \bar{A}) e^{-i\omega t} - \frac{\alpha}{2} (A^3 e^{3i\omega t} - \bar{A}^3 e^{-3i\omega t}) \right] + O(\varepsilon^2) \quad (16)$$

Furthermore, it follows from  $\dot{A}(t) = \varepsilon D_1 A + \varepsilon^2 D_2 A + \dots$  and Eqns. (12) and (14) that the reconstituted solvability condition is

$$\frac{dA}{dt} = \frac{1}{2} \varepsilon (\mu A - \alpha A^2 \bar{A}) - \varepsilon^2 \frac{i}{16\omega} (2\mu^2 A - 12\alpha\mu A^2 \bar{A} + 11\alpha^2 A^3 \bar{A}^2) + O(\varepsilon^3) \quad (17)$$

Introducing the polar transformation  $A = \frac{1}{2} a(t) e^{i\gamma(t)}$  into Eqn. (16) and setting  $\varepsilon = 1$ , without any loss of generality, we arrive at the following approximate expression for the lift coefficient:

$$C_L(t) = a(t) \cos[\omega t + \gamma(t)] - \frac{1}{4\omega} \left\{ \left[ \mu a(t) - \frac{1}{4} \alpha a(t)^3 \right] \sin[\omega t + \gamma(t)] + \frac{1}{8} \alpha a(t)^3 \sin[3\omega t + 3\gamma(t)] \right\} + \dots \quad (18)$$

Equation (18) may further be reduced to the following:

$$\begin{aligned}
C_L(t) &= a(t) \sqrt{1 + \frac{1}{16\omega^2} \left[ \mu - \frac{1}{4} \alpha a(t)^2 \right]^2} \sin[\omega t + \gamma(t) + \eta] \\
&\quad + \frac{1}{8} \alpha a(t)^3 \sin[3\omega t + 3\gamma(t)] + \dots \\
&\equiv a_1(t) \sin[\omega t + \gamma(t) + \eta(t)] + a_3(t) \sin[3\omega t + 3\gamma(t)] + \dots
\end{aligned} \tag{19}$$

where  $\eta(t) = \tan^{-1} \left[ \frac{16\omega}{\alpha a(t)^2 - 4\mu} \right]$ . Introducing the polar transformation into Eqn. (17) and setting  $\varepsilon = 1$  yields the modulation equations

$$\frac{da}{dt} = \frac{1}{8} (4\mu a - \alpha a^3) \tag{20}$$

$$\frac{d\gamma}{dt} = -\frac{1}{8\omega} \left( \mu^2 - \frac{3}{2} \alpha \mu a^2 + \frac{11}{32} \alpha^2 a^4 \right) \tag{21}$$

Setting  $\dot{a} = 0$  in Eqn. (20), we obtain  $a(4\mu - \alpha a^2) = 0$ , which gives the steady-state value of  $a$  to be either the trivial solution  $a = 0$  or  $a = 2\sqrt{\mu/\alpha}$ . For the nontrivial solution, the amplitude  $a_1$  reduces to  $a$  and the phase angle  $\eta = \pi/2$ . Hence, it follows from Eqn. (19) that

$$a_1 = \sqrt{\frac{4\mu}{\alpha}} \quad \text{and} \quad a_3 = \frac{\mu}{4\omega} \sqrt{\frac{\mu}{\alpha}} \tag{22}$$

Moreover, it follows from Eqn. (21) that the steady-state expression for  $\dot{\gamma}$  is  $-\mu^2/16$ . Consequently, the shedding frequency is given by

$$\omega_s = \omega + \dot{\gamma} = \omega - \frac{\mu^2}{16\omega} \tag{23}$$

Equation (23) shows that the van der Pol oscillator frequency  $\omega$  is not the same as the angular shedding frequency  $\omega_s$ , as predicted by the first-order expansion [21]. Consequently, an improved second-order approximate expression for the steady-state lift coefficient is

$$C_L(t) \approx a_1 \cos(\omega_s t) + a_3 \sin(3\omega_s t) \tag{24}$$

### Identification of the van der Pol Parameters

We use the CFD solver and the analytical solution of the van der Pol equation to estimate the parameters in the latter equation as follows. For a given Reynolds number, we first run the CFD

solver to calculate the time history of the lift coefficient. Second, we perform spectral analysis of the steady-state part of this time history and determine  $a_1$ ,  $a_3$ , and  $f_s$  (or  $\omega_s$ ). In Fig. 1a, we show the time history of the lift coefficient for  $Re = 10,000$  and its spectrum. Also, in Fig. 2, we show the steady-state time histories of the lift coefficients for  $Re = 200, 10,000$ , and  $100,000$ ; and in Tab. 1, we list the parameters  $a_1$ ,  $a_3$ ,  $f_s$ , and  $\omega_s$  obtained from their spectra. Third, using these values, we solve Eqns. (22) and (23) for the nonlinear and linear damping coefficients  $\alpha$  and  $\mu$  and the frequency  $\omega$ . These results are also listed in Tab. 1 for three Reynolds numbers.

Table 1. Lift parameters at different Reynolds numbers.

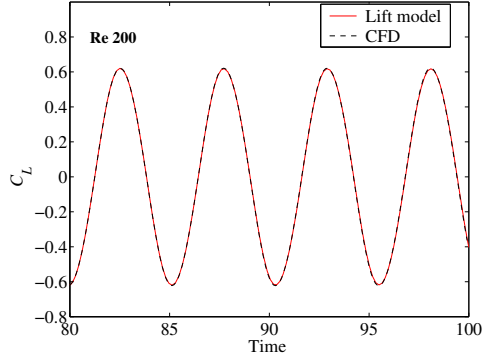
	$Re = 200$	$Re = 10,000$	$Re = 100,000$
$f_s$	0.19259	0.23898	0.25471
$a_1$	0.61470	1.79180	1.05304
$a_3$	0.00396	0.05816	0.02040
$\omega_s$	1.21008	1.50156	1.60039
$\alpha$	0.66030	0.48784	0.89603
$\mu$	0.06237	0.39156	0.24840
$\omega$	1.21028	1.50791	1.60280

Having identified all of the parameters in the van der Pol equation, we integrate it using a Runge-Kutta routine for the lift coefficient  $C_L$ . In Fig. 2, we compare the time history of the steady-state lift obtained with the CFD simulation with that obtained by integrating Eqn. (1) for three Reynolds numbers. We note that the steady-state solution of the van der Pol equation is independent of the initial conditions. It is clear that the van der Pol oscillator accurately models the CFD results for low, moderate, and high Reynolds number flows.

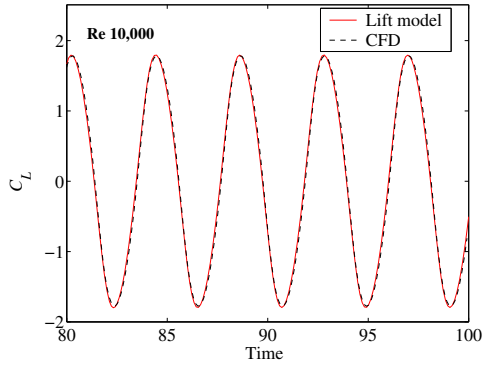
### Transient Lift

Next, we check whether the van der Pol oscillator identified using the steady-state lift can also model the transient lift. This serves two purposes. The first is that it gives confidence that we are modeling the physics correctly. The second is that we are capable of simulating the transient as well as the steady-state problem.

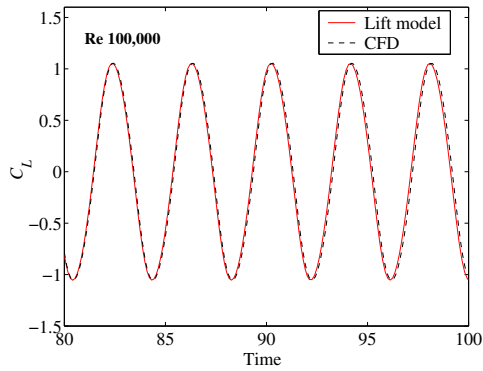
To compare the transient lift predictions of the above identified van der Pol equation with the transient lift obtained with the CFD solver, we use the values of  $\alpha$ ,  $\mu$ , and  $\omega$  obtained from the steady-state lift CFD data and integrate it using initial conditions  $C_L(t_0)$  and  $\dot{C}_L(t_0)$  corresponding to those of the transient lift



(a)  $Re = 200$



(b)  $Re = 10,000$



(c)  $Re = 100,000$

Figure 2. Comparisons between the simulated and modeled steady-state lift coefficients.

coefficient at some time  $t_0$ . Because the CFD results only yield the values of  $C_L$ , the initial values of  $\dot{C}_L$  are approximated by in-

terpolating between two points around  $t_0$  where the slope is not changing rapidly, so that any inaccuracy is minimal. In Figs. 3-5, we present the transient results for the lift coefficient obtained from the CFD code for  $Re = 200, 10,000,$  and  $100,000,$  respectively. We also present the transient solutions obtained from the van der Pol model when initiated at four different initial times.

For the case  $Re = 200,$  we simulate the transient lift using the initial starting times  $t_0 = 34, 39, 45,$  and  $50.$  We see from Fig. 3 that, the larger the starting time is, the more accurate is the model in simulating the CFD results. For example, when  $t_0 = 34,$  the van der Pol oscillator underestimates the amplitude of the lift markedly; also, there is a phase shift between its prediction and the CFD lift. These differences, however, diminish as the starting time  $t_0$  is increased, as shown in the results for  $t_0 = 50,$  which are in excellent agreement with the CFD results.

For the case  $Re = 10,000,$  we show in Fig. 4 the predicted transient lift using the initial starting times  $t_0 = 12, 14, 16,$  and  $18.$  And for the case  $Re = 100,000,$  we show in Fig. 5 the predicted transient lift using the initial starting times  $t_0 = 10, 12, 14,$  and  $16.$  It follows from Figs. 4 and 5 that the discrepancy in modeling the lift amplitude for moderate and high Reynolds number flows is resolved. However, there is still a phase difference between the two results, which again is minimized by using larger starting times.

One possible explanation for these deviations is the fact that the CFD results contain two types of transients: those arising physically and those arising from numerical analysis effects (e.g., impulsive initial conditions). It seems that the rate of decay of the latter depends on the Reynolds number. We note from Figs. 3-5 that the larger the Reynolds number is, the faster is the rate of convergence to the physical solution. For  $Re = 200,$  it follows from Fig. 3 that the transients due to numerical effects in the CFD simulation might propagate for some time after the initial conditions and might take up to 50 time units to decay completely. On the other hand, for  $Re = 10,000$  and  $Re = 100,000,$  it follows from Figs. 4 and 5 that the transients due to numerical effects decay much faster, possibly lasting for about 18 and 16 time units, respectively.

Clearly, the agreement between the van der Pol and CFD results is excellent once the transients arising from numerical effects have died out. Therefore, the van der Pol oscillator can model both of the steady-state and transient lifts on a cylinder in a uniform flow.

## SUGGESTED DRAG MODEL

Currie and Turnbull [13] proposed a model for the drag similar to the lift-wake oscillator proposed by Hartlen and Currie [12] who represented the lift by the Rayleigh equation. To study resonant responses of suspended elastic cables, Kim and Perkins [20] modeled the lift by a van der Pol equation with frequency  $f_s$  and the drag with another van der Pol equation with frequency

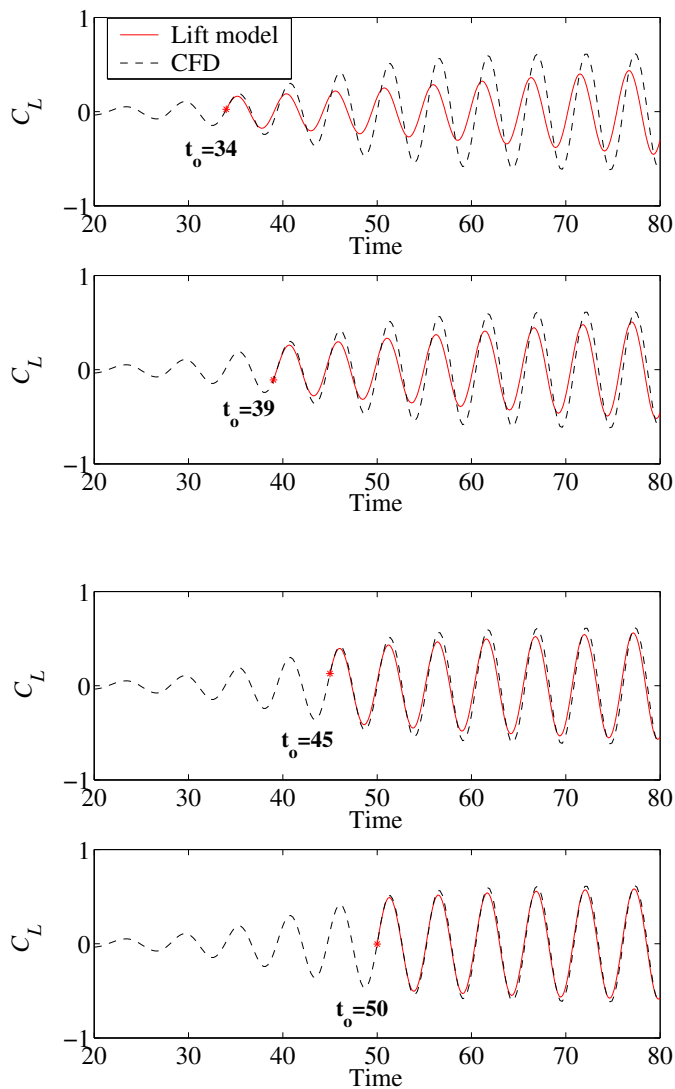


Figure 3. Simulated and modeled transient lift coefficients for different starting times for  $Re = 200$ .

$2f_s$  and coupled the two equations nonlinearly. These couplings were introduced based on the fact that the main frequency of the drag component is twice the main frequency of the lift component. Qin [26] proposed a drag model that has a linear term and a quadratic term in the lift.

Because the drag and lift are the result of the pressure distribution on the surface of the cylinder, it is feasible to relate the drag to the lift directly. The drag consists of two components: the first is a mean component independent of the lift and the second is a periodic component related to the unsteady periodic lift. The fact that the major component in the spectrum of the drag

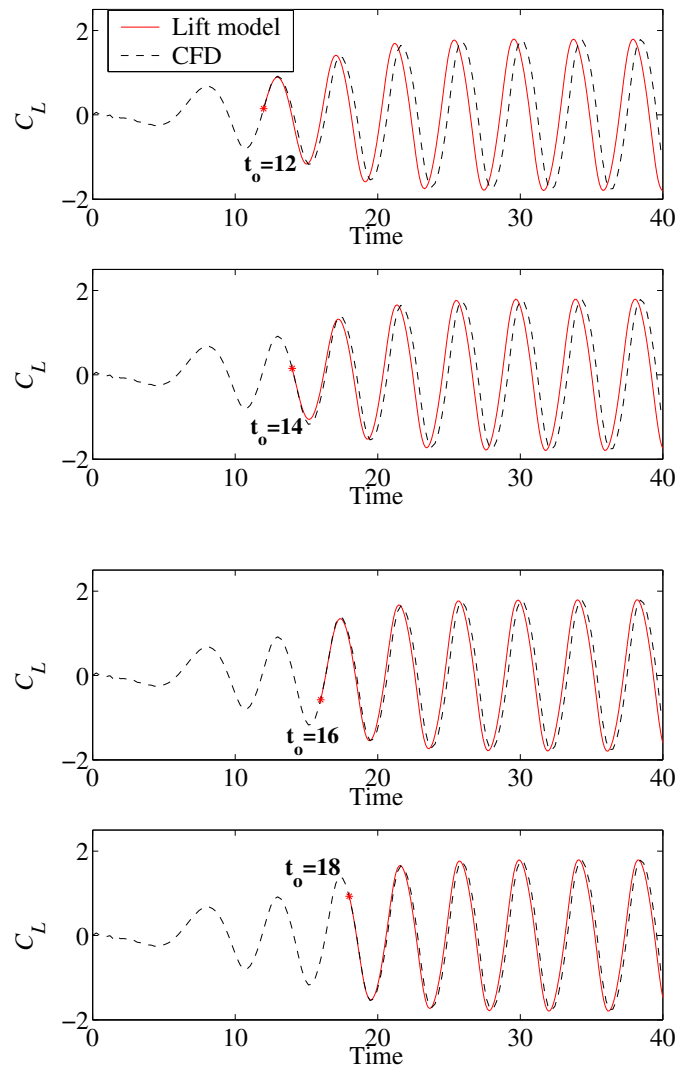


Figure 4. Simulated and modeled transient lift coefficients for different starting times for  $Re = 10,000$ .

coefficient is at twice the shedding frequency, as illustrated in Fig. 1b, suggests that the drag is a quadratic function of the lift; that is, the drag is proportional to either  $C_L^2$ ,  $\dot{C}_L^2$ , or  $C_L\dot{C}_L$ . Of these three forms, the correct form must yield the right phase relation between the drag and the lift. As shown in Hajj et. al. [27], this phase can be measured as the phase of the cross bispectrum between  $2f_s$  in the drag and  $f_s$  in the lift.

Based on the analysis of the CFD solutions, Nayfeh et al. [21] found that the phase relation between the periodic drag component and the lift to be near  $3\pi/2$  in all records. From that, they concluded that the periodic component of the drag must be proportional to  $-C_L\dot{C}_L$ . Consequently, the drag coefficient  $C_D(t)$  is

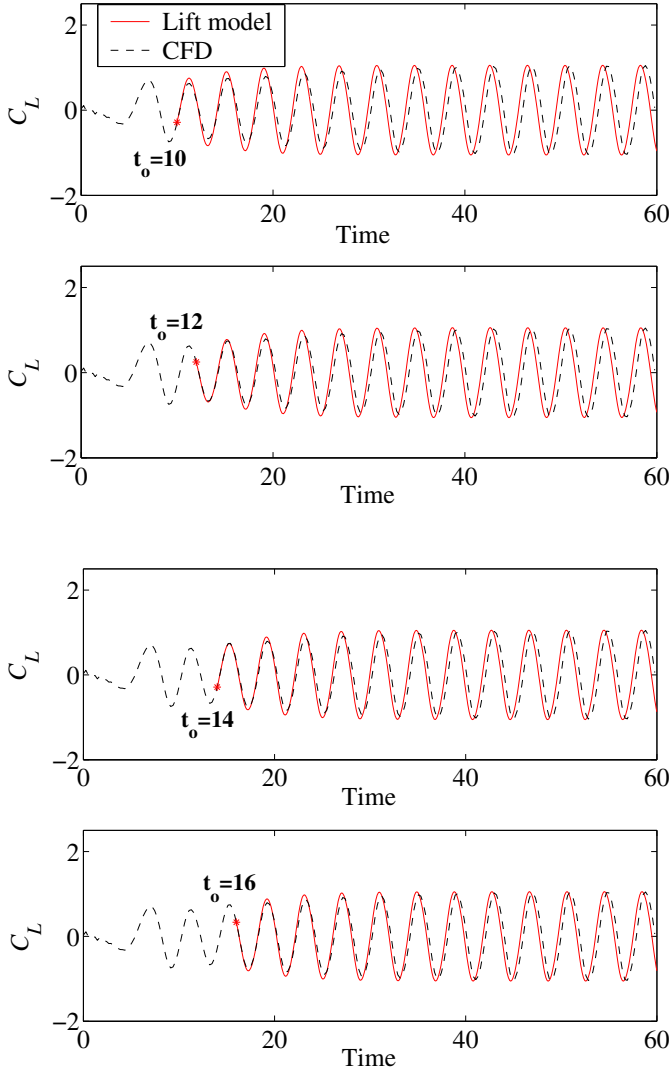


Figure 5. Simulated and modeled transient lift coefficients for different starting times for  $Re = 100,000$ .

modeled as

$$C_D(t) = \bar{C}_D - 2 \frac{a_2}{\omega_s a_1^2} C_L(t) \dot{C}_L(t) \quad (25)$$

where  $\bar{C}_D$  is the mean component of drag, which is constant for steady-state behavior but time-dependent for transient behavior, and  $a_2$  is the amplitude of the drag component at  $2f_s$ . The value of  $\bar{C}_D$  is determined from the CFD steady-state time history of the drag and the value of  $a_2$  is determined its spectral analysis. In Tab. 2, we present their values for the three Reynolds numbers  $Re = 200, 10,000, \text{ and } 100,000$ .

Table 2. Drag model parameters at different Reynolds numbers.

	$Re = 200$	$Re = 10,000$	$Re = 100,000$
$a_2$	0.0369	0.1291	0.0623
$\bar{C}_D$	1.18	1.62	0.85

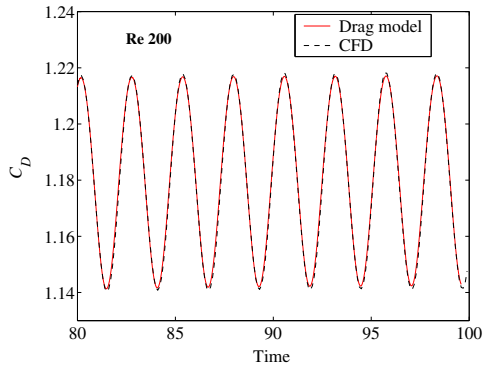
### Steady-State Drag

The van der Pol equation for the lift coefficient is first integrated to evaluate the steady-state  $C_L(t)$  and  $\dot{C}_L(t)$ . Then, Eqn. (25) is used to evaluate the drag coefficient  $C_D(t)$ . In Fig. 6, we compare the results obtained from the model with the CFD results for the three Reynolds numbers  $Re = 200, 10,000, \text{ and } 100,000$ . It follows from Fig. 6a for  $Re = 200$  that there is excellent agreement between the two solutions. Moreover, it follows from Figs. 6b and 6c for  $Re = 10,000$  and  $Re = 100,000$  that the agreement is good. The small deviation appears to be more amplified at  $Re = 10,000$  and could be attributed to the fact that the CFD results (both the spectrum in Fig. 1b and time history in Fig. 6b) show the drag coefficient to be modulated. This aspect of the drag does not seem to be completely modeled by Eqn. (25).

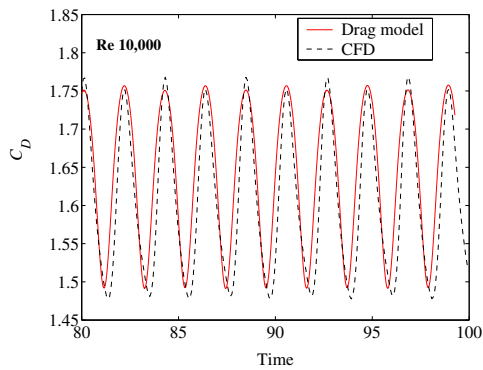
### Transient Drag

As with the proposed lift model, we also examine the capability of drag model to predict the transient drag with the parameter values in Tabs. 1 and 2 obtained using the steady-state lift and drag. We first integrate the van der Pol equation for the lift coefficient with initial conditions  $C_L(t_0)$  and  $\dot{C}_L(t_0)$  in the transient regions. Then, we use the outcome in Eqn. (25) to calculate the drag coefficient. However, because the mean drag  $\bar{C}_D$  is time-dependent in the transient region, modeling it as a constant following the steady-state results brings about a mismatch with the CFD solution. To avoid this, we extracted the transient profile of the mean drag from the CFD simulation as a function to replace the constant value of  $\bar{C}_D$  in Eqn. (25). Hence, both of the analytical and CFD solutions exhibit the same trend when plotted together. In other words, Eqn. (25) with  $\bar{C}_D$  being constant models fully the steady-state drag, models the fluctuating part of the transient drag, but does not model the mean part of the transient drag.

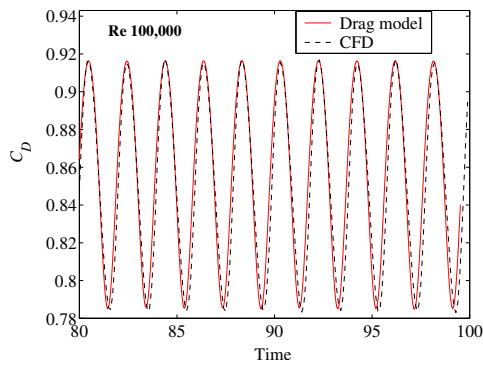
In Figs. 7-9, we present results from the CFD code and the drag model for the three Reynolds numbers  $Re = 200, 10,000, \text{ and } 100,000$ . Again, we find that, in general, the accuracy of the proposed model improves for later starting times. For the low Reynolds number flow in Fig. 7, we find that the proposed model underestimates the amplitude of  $C_D$  when starting at  $t_0 = 40$ , but it does an excellent job when starting at  $t_0 \geq 60$ , which is still in the transient region. For the moderate and high Reynolds number flows in Figs. 8 and Figs. 9, respectively, we find that the model



(a)  $Re = 200$



(b)  $Re = 10,000$



(c)  $Re = 100,000$

Figure 6. Comparisons between the simulated and modeled steady-state drag coefficients.

does an excellent job in predicting the amplitude of  $C_D$ ; however, there exists a small phase difference between the two solutions.

This conclusion is similar to the conclusion for the transient lift. This is expected because the drag model is based on the lift model. We recall that transients due to the numerical effects in the modeled lift at  $Re = 200$  decay after 50 time units, whereas they decay after 18 and 16 time units for  $Re = 10,000$  and  $Re = 100,000$ , respectively. Therefore, the agreement between the drag model and the CFD results is excellent once the transients arising from the numerical effects have died out.

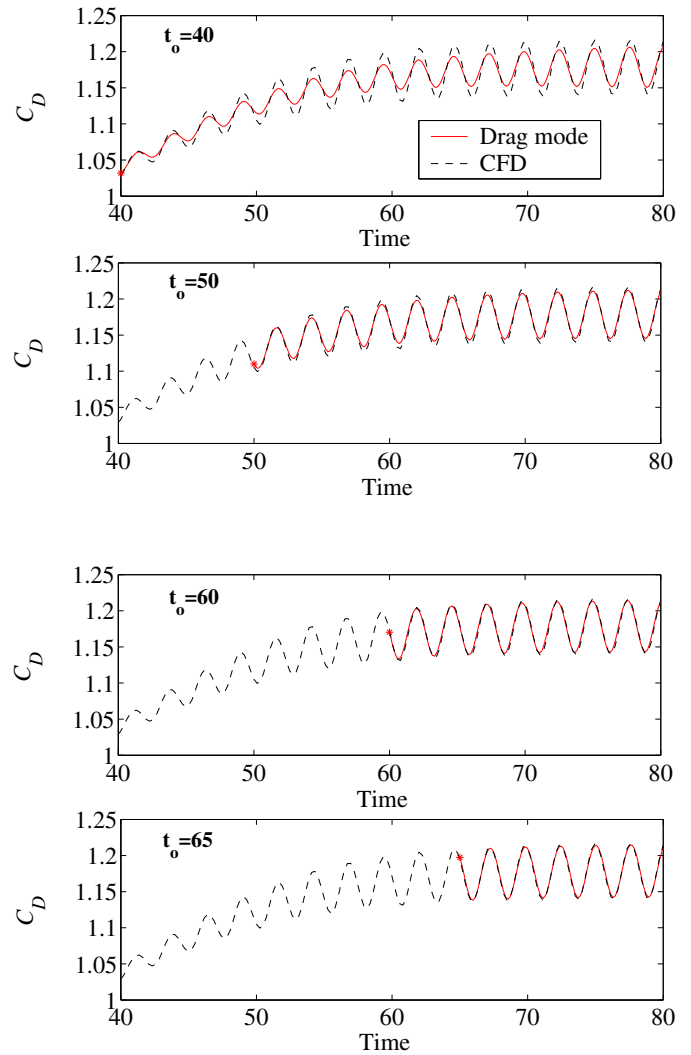


Figure 7. Simulated and modeled transient drag coefficients for different starting times for  $Re = 200$ .

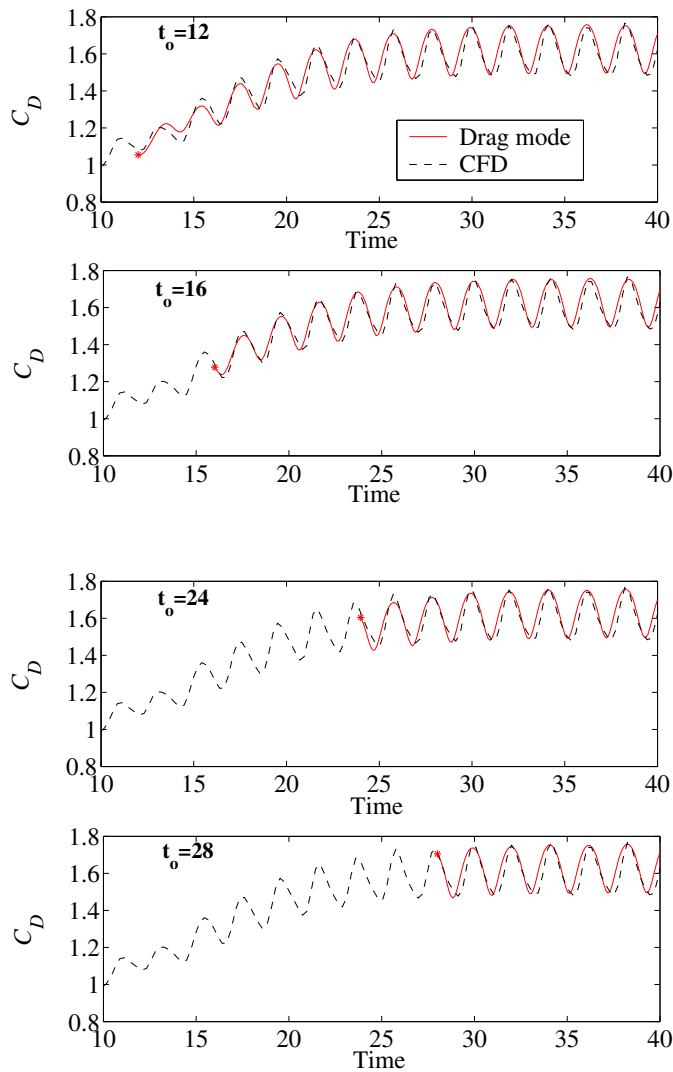


Figure 8. Simulated and modeled transient part of the drag coefficients for different starting times for  $Re = 10,000$ .

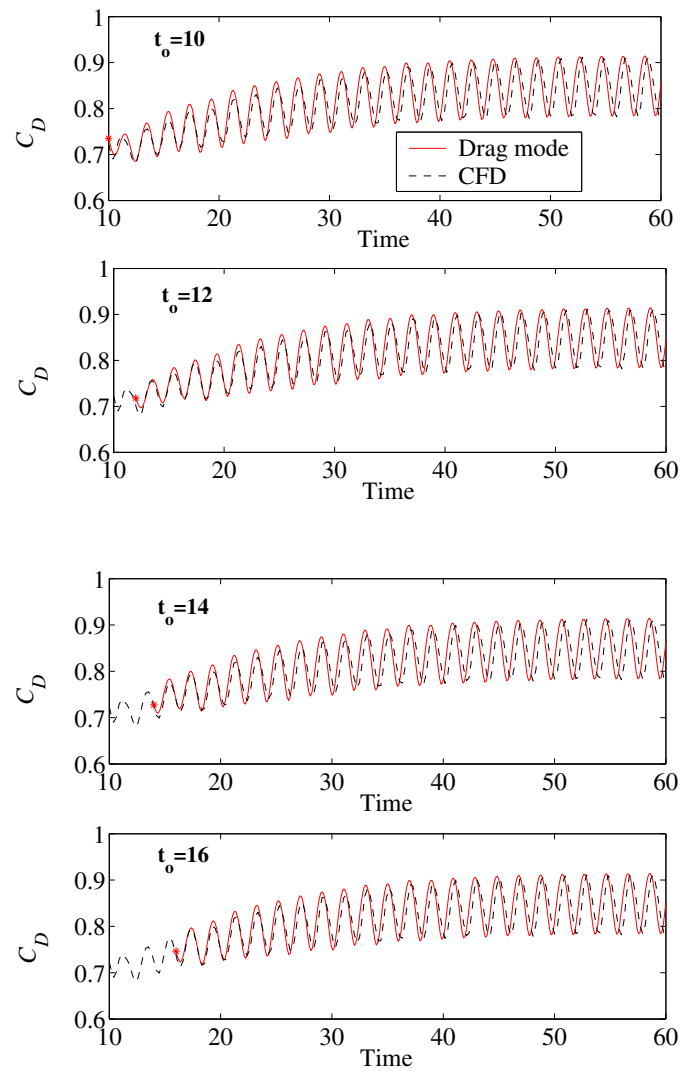


Figure 9. Simulated and modeled transient part of the drag coefficients for different starting times for  $Re = 100,000$ .

## CONCLUSIONS

Lift and drag coefficients for the two-dimensional flow over a stationary circular cylinder were modeled. The model accounts for the coupling between these coefficients and covers the steady-state and transient behaviors. This simple but efficient model is based on representing the lift coefficient by the van der Pol equation. Furthermore, the drag coefficient is represented by a mean drag term and a nonlinear term proportional to the lift coefficient times its time derivative. The parameters for this model were obtained by matching a second-order approximate solution of the van der Pol equation with the CFD steady-state lift. The latter was obtained by numerically integrating the unsteady Reynolds-

averaged Navier-Stokes equations (RANS). The numerical simulations utilize the artificial compressibility concept by introducing an artificial pressure unsteadiness term in the continuity equation.

Numerical simulations were carried out for several Reynolds numbers, representing a wide range of flows. Here, we present results and comparisons for the three Reynolds numbers:  $Re = 200$ ,  $Re = 10,000$ , and  $Re = 100,000$ . For the steady-state lift and drag coefficients, we found that the model does an excellent job in matching the CFD results. As for the transient lift and drag coefficients, we found that the accuracy of the model depends on the starting point at which the initial conditions are

taken. The closer the starting point is to the steady-state part, the more accurate is the prediction of the model. In summary, the model can be used reliably to predict the steady-state as well as the transient lift and drag coefficients.

## ACKNOWLEDGMENT

This work was supported by Vetco Gray and Starmark Offshore Inc., David W. Hughes and Robert Sexton, Technical Monitors.

## REFERENCES

- [1] Bishop, R. E. D., and Hassan, A. Y., 1964. "The lift and drag forces on a circular cylinder oscillating in a flowing fluid". *Proceedings of the Royal Society of London, Series A*, **277**, pp. 32–50.
- [2] Bishop, R. E. D., and Hassan, A. Y., 1964. "The lift and drag forces on a circular cylinder oscillating in a flowing fluid". *Proceedings of the Royal Society of London, Series A*, **277**, pp. 51–75.
- [3] Ferguson, N., and Parkinson, G. V., 1967. "Surface and wake flow phenomena of the vortex-excited oscillation of a circular cylinder". *Journal of Engineering for Industry*, **89**, pp. 831–838.
- [4] Williamson, C. H. K., and Roshko, A., 1988. "Vortex formation in the wake of an oscillating cylinder". *Journal of Fluids and Structures*, **2**, pp. 355–381.
- [5] Sarpkaya, T., and Shoaff, R. L., 1979. "Numerical modeling of vortex-induced oscillations". In *Proceedings of the Specialty Conference: Civil Engineering in the Oceans IV*, Vol. **1**, pp. 504–517.
- [6] Sarpkaya, T., and Shoaff, R. L., 1979. "Inviscid model of two-dimensional vortex shedding by a circular cylinder". *AIAA Journal*, **17**, pp. 1193–1200.
- [7] Mittal, R., and Balachandar, S., 1995. "Effect of three-dimensionality on the lift and drag of nominally two-dimensional cylinders". *Physics of Fluids*, **7**, pp. 1841–1865.
- [8] Al-Jamal, H., and Dalton, C., 2004. "Vortex induced vibrations using large eddy simulation at a moderate reynolds number". *Journal of Fluids and Structures*, **19**, pp. 73–92.
- [9] Sarpkaya, T., 1979. "Vortex-induced oscillations". *Journal of Applied Mechanics*, **46**, pp. 241–258.
- [10] Billah, K. Y., 1989. "A Study of Vortex-Induced Vibration". PhD Thesis, Princeton University, Princeton, NJ.
- [11] Blevins, R. D., 1990. *Flow-Induced Vibration*. Van Nostrand Reinhold, New York, NY.
- [12] Hartlen, R. T., and Currie, I. G., 1970. "Lift-oscillator model of vortex-induced vibration". *ASCE Journal of the Engineering Mechanics Division*, **96**, pp. 577–591.
- [13] Currie, I. G., and Turnball, D. H., 1987. "Streamwise oscillations of cylinders near the critical reynolds number". *Journal of Fluids and Structures*, **1**, pp. 185–196.
- [14] Iwan, W. D., and Blevins, R. D., 1974. "A model for vortex-induced oscillation of structures". *Journal of Applied Mechanics*, **41**, pp. 581–586.
- [15] Skop, R. A., and Griffin, O. M., 1973. "A model for the vortex-excited resonant response of bluff cylinders". *Journal of Sound and Vibration*, **27**, pp. 225–233.
- [16] Skop, R. A., and Balasubramanian, S., 1995. "A nonlinear oscillator model for vortex shedding from a forced cylinder. part 1: Uniform flow and model parameters". *International Journal of Offshore and Polar Engineering*, **5**, pp. 251–255.
- [17] Skop, R. A., and Balasubramanian, S., 1995. "A nonlinear oscillator model for vortex shedding from a forced cylinder. part 2: Shear flow and axial diffusion". *International Journal of Offshore and Polar Engineering*, **5**, pp. 256–260.
- [18] Billah, K. Y., and Ahmad, O., 2003. "Vortex-induced vibration structural response under parametric excitation". In *Proceedings of the IUTAM Symposium on Integrated Modeling of Fully Coupled Fluid Structure Interactions Using Analysis, Computations and Experiments*, Vol. **1**, pp. 279–288.
- [19] Skop, R. A., and Balasubramanian, S., 1997. "A new twist on an old model for vortex-excited vibrations". *Journal of Fluids and Structures*, **11**, pp. 395–412.
- [20] Kim, W. J., and Perkins, N. C., 2002. "Two-dimensional vortex-induced vibration of cable suspensions". *Journal of Fluids and Structures*, **16**, pp. 229–245.
- [21] Nayfeh, A. H., Owis, F., and Hajj, M. R., 2003. "A model for the coupled lift and drag on a circular cylinder". In *Proceedings of DETC'03, ASME 2003 Design Engineering Technical Conferences and Computers and Information in Engineering Conference*. DETC2003/VIB-48455.
- [22] Spalart, P. R., and Allamras, S. R., 1992. "A one-equation turbulence model for aerodynamic flows". In *Proceedings of the AIAA 30th Aerospace Sciences Meeting and Exhibit*. AIAA paper 92-0439.
- [23] Spalart, P. R., and Allamras, S. R., 1994. "A one-equation turbulence model for aerodynamic flows". *La Recherche Aerospaciale*, **1**, pp. 5–21.
- [24] Nayfeh, A. H., 1973. *Perturbation Methods*. Wiley, New York, NY.
- [25] Nayfeh, A. H., 1981. *Introduction to Perturbation Techniques*. Wiley, New York, NY.
- [26] Qin, L., 2004. "Development of Reduced-Order Models for Lift and Drag on Oscillating Cylinders with Higher-Order Spectral Moments". PhD Thesis, Virginia Polytechnic Institute and State University, Blacksburg, VA.
- [27] Hajj, M. R., Miksad, R. W., and Powers, E. J., 1993. "Fundamental-subharmonic interaction: Effect of phase relations". *Journal of Fluid Mechanics*, **256**, pp. 403–426.